Case Report

JVC Journal of Veterinary Clinics

pISSN 1598-298X • eISSN 2384-0749
J Vet Clin 2023;40:375-381
https://doi.org/10.17555/jvc.2023.40.5.375

Check for updates

Contrast Enhanced Ultrasonography and CT Features of Gastrointestinal Stromal Tumor in a Dog

Saran Chhoey[1,2]
Soyeon Kim[3,4]
Kroesna Kang[2]
Sath Keo[2]
Jihye Choi[3,*]

[1]Graduate School, Royal University of Agriculture, Phnom Penh 12401, Cambodia
[2]Faculty of Veterinary Medicine, Royal University of Agriculture, Phnom Penh 12401, Cambodia
[3]Department of Veterinary Medical Imaging, College of Veterinary Medicine, Seoul National University, Seoul 08826, Korea
[4]Department of Veterinary Medical Imaging, College of Veterinary Medicine, Chonnam National University, Gwangju 61186, Korea

*Correspondence: imsono@snu.ac.kr

ORCID
Saran Chhoey:
https://orcid.org/0000-0001-7427-6024
Soyeon Kim:
https://orcid.org/0000-0001-8819-9576
Kroesna Kang:
https://orcid.org/0000-0002-6818-1982
Sath Keo:
https://orcid.org/0000-0003-0056-647X
Jihye Choi:
https://orcid.org/0000-0002-1258-7158

Abstract A large abdominal mass was incidentally found in a 13-year-old mixed-breed dog and was confirmed to be a cecal gastrointestinal stromal tumor (GIST). Contrast-enhanced ultrasound and post-contrast computed tomography (CT) showed mild contrast enhancement of the mass, indicating low blood flow. The tumor origin was determined to be the cecum by identifying the vessels supplying the mass on post-contrast CT. The exophytic growth of the tumor left the cecal lumen intact without obstruction. This report described the CEUS and CT perfusion of the cecal GIST and perfusion evaluation can help diagnose and characterize GISTs in dogs.

Key words blood flow, canine, cecal tumor, CEUS, computed tomography.

Received September 12, 2023 / Revised October 20, 2023 / Accepted October 20, 2023

Introduction

Gastrointestinal stromal tumors (GISTs), leiomyomas, and leiomyosarcomas are mesenchymal tumors of the gastrointestinal (GI) tract (1). GISTs originate from the submucosa, particularly from Cajal cells and found in the small intestine (duodenum, jejunum, ileum) and large intestine (colon and cecum) in dogs (1,3,15). Clinical signs depend on the size, growth pattern, and location of the tumor. Human patients with GISTs commonly present with abdominal pain and distention and mucosal ulceration associated with GI bleeding (3,5). However, the exophytic and cavitary nature of GISTs may delay luminal constriction and the onset of symptoms (3,11,15).

Ultrasonography is a commonly used imaging modality for GI tumors in veterinary medicine to assess the location, size, echogenicity, and homogeneity of the mass, thickness, layering, and motility of the wall, the luminal content, vascularity, presence of cavitation, and evidence of perforation or ulceration and adjacent structures such as lymph nodes and peritoneum; nonetheless, luminal gas can limit the acoustic window by generating acoustic shadowing and hyperechoic reverberation artifacts (3,5,15,18,22). Only a few veterinary studies have presented the ultrasonographic findings of GI mesenchymal tumors, such as leiomyomas and leiomyosarcomas, which are usually found as smooth muscle tumors that tend to be larger than 3 cm, with intramural lesions that develop from the serosa as large, eccentric masses (1,3,7,18). Large leiomyosarcomas can be heterogeneous, with a mixed echogenic pattern (1,19). The presence of anechoic and hypoechoic areas within the mass on ultrasonography may be correlated with central degeneration and necrosis in dogs (1,15,19).

Contrast-enhanced ultrasonography (CEUS) is used to evaluate the contrast patterns and tissue perfusion of GI tumors in human patients, especially gastric carcinoma and intestinal lymphoma. Human studies have shown that CEUS has higher sensitivity than computed tomography (CT) for detecting blood flow in hypovascularized lesions (15,20,22). Other human studies used contrast-enhanced harmonic endoscopic ultrasonography for the early diagnosis of GISTs based on tumor blood flow and the positive sampling rate is higher in CEUS-guided biopsy than in conventional ultrasound-guided biopsy for detecting GISTs (2,22). However, veterinary studies performed CEUS of the GI tract in a few animals, including 14 healthy dogs, 26 dogs with chronic inflammatory enteropathy, and seven dogs with intestinal lymphoma (4,20,22).

Computed tomography (CT) can be used for determination of the tumor location and extent, the diagnosis and staging of GI tumors (14,24). Usefulness of CT for evaluating the sites, contrast enhancement pattern, and local extent of the mass and metastases was revealed in a previous canine study including gastric lymphoma, adenocarcinoma, inflammatory polyps, and leiomyoma (24). The study presented the possibility for differentiation gastric lymphoma from other tumors based on the CT attenuation values of the mass. Recently, CT features of the small intestinal tumors was reported in a large population of 37 dogs with adenocarcinoma, lymphoma, and spindle cell sarcoma and the authors determined usefulness of the contrast CT characteristics in differentiating small intestinal adenocarcinomas, lymphomas, and spindle cell sarcoma in dogs (14). However, there was no study focusing on the CEUS and CT features of GIST in a dog. Therefore, herein, we describe CEUS and CT findings of a canine GIST originating from the cecum.

Case Report

A 13-year-old neutered male, weighing 5.39 kg, mixed breed dog was presented for evaluation of an abdominal mass incidentally found during radiography at a local animal clinic for a bite injury that occurred approximately 10 days before presentation. The dog was asymptomatic except for pain at the bite site and rib fractures. Abdominal palpation during physical examination detected elevated abdominal pressure and distension.

Abdominal radiography was performed using a digital radiographic system, EVA-HF525 (Gemss-Medical; Seongnam, Korea) with a maximum tube voltage of 125 KV and maximum tube current of 500 mA with a cesium-iodine-based flat panel detector, FDX4343R (Gemss-Medical; Seongnam, Korea) integrated into the table. Abdominal radiography revealed a round soft tissue mass in the ventral part of the middle abdomen (Fig. 1). The large mass, approximately 10 cm × 17 cm × 14 cm in size, displaced the gas-filled intestines, and colon to the left and caudodorsal directions and the right kidney and stomach to the cranial direction. The cranial margin of the mass was clear; however, the caudal margin of the mass was effaced with the adjacent colon and small intestine. Multiple calculi were observed bilaterally in the kidneys, bladder, prostate, and urethra.

Conventional ultrasonography was performed using an ultrasound machine, Prosound Alpha 7 (Hitachi-Aloka; Tokyo, Japan) with a 10 MHz linear transducer. The large mass occupied most of the right abdomen, from the caudal border of the liver to the cranial border of the bladder, displacing the small and large intestines to the left side (Fig. 2A-E). The mass showed a mixed echotexture consisting of hyperechoic parenchyma and multiple hypoechoic areas. On color and power Doppler modes, blood flow signals detected within

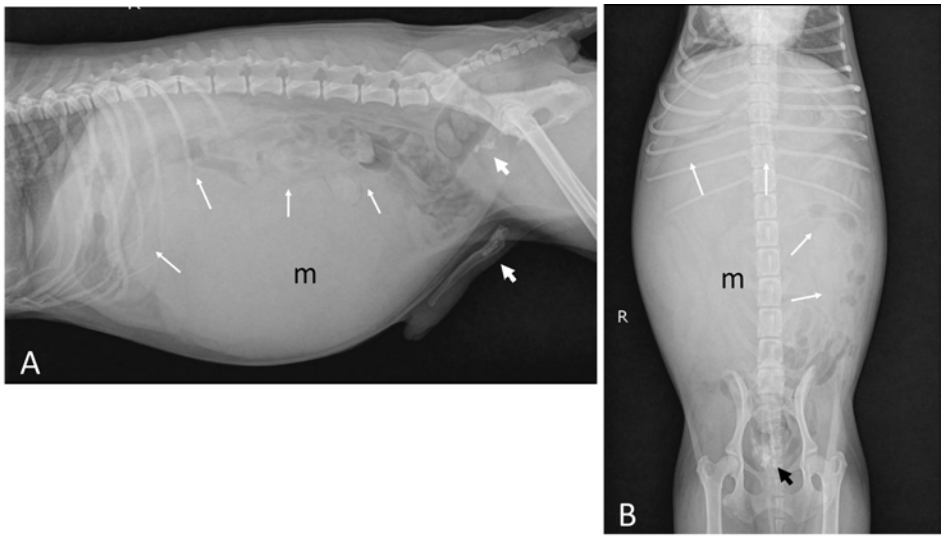

Fig. 1. Abdominal radiography of the dog. On the lateral view (A), a large mass (m) in the ventral side of the middle abdomen displaced the right kidney and stomach to the cranial direction and the gas-filled intestines, and colon to the caudodorsal direction (long arrows). On the ventrodorsal view (B), the mass (m) occupied most of the right middle abdomen, displacing the intestinal loops to the left side (long arrows). The caudal margin of the mass was indistinct from the colon and small intestines. Multiple calculi (short arrows) were observed in the bilateral kidneys, bladder, and urethra.

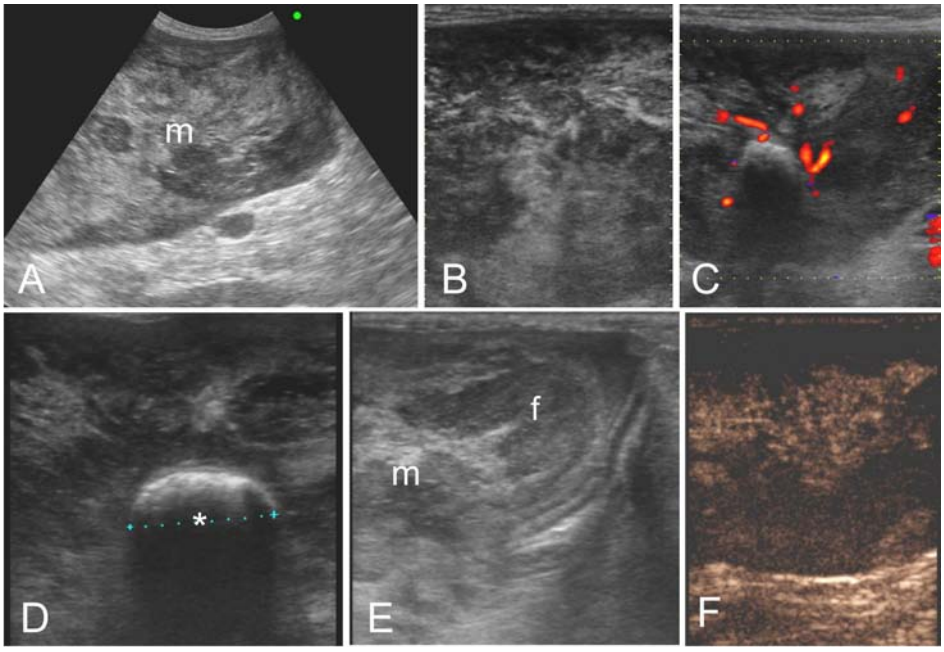

Fig. 2. Conventional ultrasonography (A-E) and contrast-enhanced ultrasonography (E) of the large mass. (A, B) The mass (m) had a mixed echotexture consisting of hyperechoic parenchyma and multiple hypoechoic areas. The margin of the mass was slightly irregular but clear. (C) On power Doppler imaging, the blood flow signal was detected within the mass. (D) The involvement of the intestinal loops (asterisk) was suspected; however, the large size of the mass prevented determining its origin. (E) Hyperechoic change of the abdominal fat and a small amount of peritoneal effusion (f) were found surrounding the mass. (F) Enhancement was heterogenous on contrast-enhanced ultrasonography.

the mass. The margins of the mass were slightly irregular but clear. The involvement of the ileocecocolic junction and some small intestinal loops was suspected, and the primary tumor originated from the GI tract; however, the large size of the mass prevented determining its origin. Hyperechoic changes in the abdominal fat and a small amount of peritoneal effu-

sion were observed around the mass. Multiple hypoechoic nodules, about 3-12 mm in diameter, were observed in the liver. A nodule (4.6 × 4.0 mm) with a hyperechoic center and a hypoechoic margin was detected in the spleen. Multiple calculi were found in the urinary system; however, there was no evidence of urinary tract obstruction.

CEUS of the abdominal mass was performed after injecting a microbubble contrast agent (SonoVue™; Bracco Imaging, Milano, Itary). After agitation, 0.5 mL of the contrast agent was administered by rapid bolus injection into the cephalic vein using a 24-gauge catheter via a 3-way stopcock, followed by rapid bolus injection of 5 mL of 0.9% sodium hydrochloride solution. The transmitted energy was reduced to magnitudes of 7%, and the mechanical index was set to 0.07. In the extended pure harmonic detection mode, the focus point was set at the bottom for homogeneous energy distribution over the entire image. After the contrast injection, a relatively distinct contrast enhancement of the mass was observed throughout the parenchyma, with several unenhanced areas (Fig. 2F). The large size of the mass prevented identifying its origin; however, intestinal origin was suspected because there was no anatomical connection between the mass and adjacent viscera and blood flow to the mass was low. Multiple nodules in the liver were homogeneously enhanced, and contrast enhancement and wash-in and wash-out times were similar to those of the normal hepatic paren-

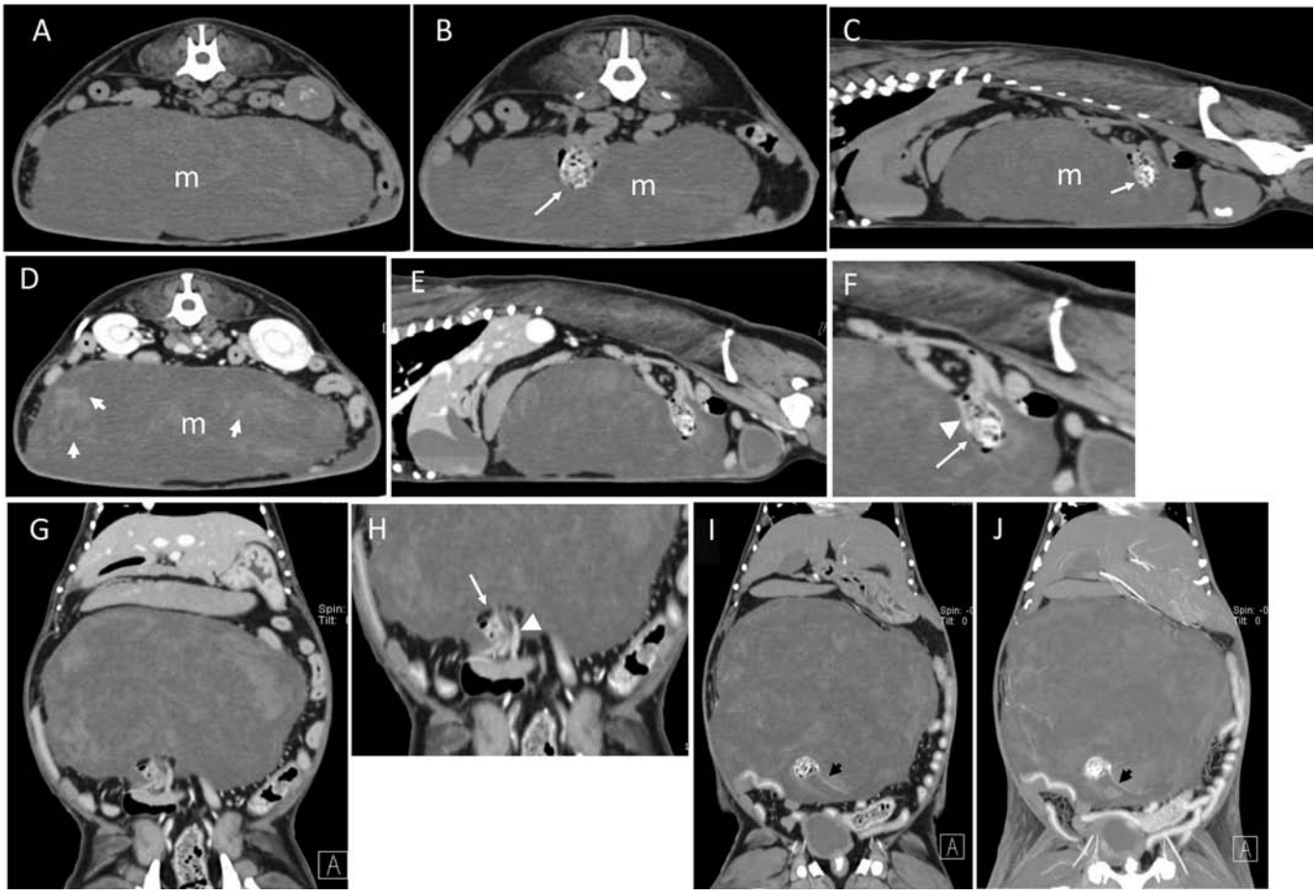

Fig. 3. Pre- and post-contrast computed tomography (CT) of the mass. On the transverse (A, B) and sagittal (C) planes of pre-contrast CT images, a large mass (4.5 × 15.0 × 11.9 cm) with soft tissue density was found in the mid-abdomen, displacing the liver and spleen cranially and the intestinal loops dorsally and to the left. The mass was hypoattenuating (18 HU) and contained a slightly hyperattenuating region (34 HU). An intestinal loop (long white arrow) was found at the dorsal periphery of the mass. On the post-contrast CT images (D-J), mild contrast enhancement of the mass with multiple hyperattenuating regions (short white arrows) was observed. On the transverse (E) and sagittal (G) planes, the continuation of the intestinal loop (long arrows) involved in the mass with the enhanced mucosa of the ileum (arrowhead) was observed, which was more evident in the magnified images (F, H). The vessels supplying the mass (black arrow) were detected on the dorsal plane of a post-contrast image (I) and a maximum-intensity projection image (J). Cystic calculi are clearly visible. The left side of the transverse and dorsal planes is the right side of the dog, and the left side of the sagittal plane is the cranial side of the dog. Window level, 40 HU; window width, 400 HU.

chyma on CEUS. Benign nodular hyperplasia was considered. The splenic nodule showed homogeneous enhancement, similar to that of the normal splenic parenchyma, and metastasis was unlikely.

CT was performed to determine the origin of the mass, treatment planning, and investigate the evidence of tumor metastasis. CT scans were acquired using a 16-slice CT scanner, Siemens Emotion 16 (Siemens; Forchheim, Germany) with the following settings: slice thickness, 1 mm; pitch, 0.8; rotation duration, 600 ms; tube voltage, 120 kV; and tube current, 130 mA. A contrast study was performed after injecting 600 mg I/kg of iohexol (Omnipaque 300®; GE Healthcare, Chicago, IL, USA) at a rate of 3.0 mL/sec using a power injector, Medrad Vistron CT injection system (MedRad; Warrendale, PA, USA) through 24-gauge intravenous catheters. CT images were evaluated in soft tissue window setting (window level of 40 Hounsfield units [HU] and window width of 400 HU) and bone window setting (window level of 450 HU and window width of 1500 HU). On the pre-contrast CT images, a large mass (approximately 4.5 × 15.0 × 11.9 cm) with soft tissue density was found in the mid-abdomen, displacing the liver and spleen cranially and the intestinal loops dorsally and to the left (Fig. 3). The mass was hypoattenuated (approximately 18 HU) and contained a slightly hyperattenuated region (approximately 34 HU). An intestinal loop was found within the dorsal periphery of the mass, and the wall of the involved intestine was not distinguished from the mass parenchyma. The intestinal lumen within the mass was maintained without narrowing. On the post-contrast CT images, contrast enhancement of the mass was observed in the hypoattenuating parenchyma (24 HU) and the internal hyperattenuating region (59-78 HU). The mass received blood flow from the ileocolic artery arteries branching from the cranial mesenteric artery; therefore, the mass was determined to be of a cecal origin. Mild fat stranding and mild peritoneal effusion were observed around the mass. The cranial mediastinal lymph nodes were mildly enlarged (8.8 × 5.0 mm); however, there was no evidence of metastasis.

The abdominal mass was of cecal origin based on imaging features. GIST was tentatively diagnosed based on the exophytic proliferative pattern of the mass and adenocarcinoma, leiomyosarcoma and lymphoma should be differentiated. The mass was confirmed to be a cecal GIST via laparotomy and histopathological examination. The dog was recovered uneventfully.

Discussion

This report is the first to describe CEUS and CT findings of a cecal GIST in a dog. GIST showed mild contrast enhancement on CEUS and CT, indicating low blood flow to mesenchymal tumors. The large size of the mass prevented assessing its origin and anatomical relationship with adjacent organs; however, the tumor origin was determined to be the cecum by identifying the vessels supplying the mass on post-contrast CT images. The cecal lumen was intact without narrowing or obstruction due to the exophytic characteristics of the GIST.

It is difficult to be certain whether hypoperfusion of the mass of the present case is typical of GISTs in dogs because no studies performed CEUS of GISTs in veterinary medicine. Meanwhile, in humans, GISTs are usually hypervascular with arterial hyperenhancement in most cases on CEUS and post-contrast CT (1,19,20,25). These perfusion features can help distinguish GISTs from other subepithelial lesions (10,17). Although hypervascularity is a common feature of GISTs in humans, perfusion patterns on CEUS and CT vary depending on tumor size, location, presence of necrosis, and disease stage and can displays avascular areas (2,18,19). Considering the large size of the GIST in our case, the discrepancy in the perfusion features between our case and human studies may be related to the large size of the mass and the presence of large necrotic areas within the mass. Similarly, most human patients with GIST (88%) presented lesions with avascular necrosis (3,13,15,18).

The perfusion of GISTs may provide valuable information for treatment decisions and the early prediction of tumor response to treatment in human patients with GIST. In particular, baseline perfusion features of GIST significantly predict the efficacy of imatinib therapy (13). Moreover, changes in tumor vascularity and enhancement patterns over time after imatinib treatment can indicate the effectiveness of tumor control (13).

Several human and veterinary studies have shown that GI tumor growth patterns vary depending on tumor type and location. In dogs, intestinal adenocarcinoma is usually characterized by diffuse or focal wall thickening with thickening of the submucosal layer or muscular layer and hypoechoic change that can obstruct the GI lumen and cause clinical symptoms such as vomiting, anorexia, and weight loss (3,5,10,19,22). Intestinal lymphoma in dogs usually shows transmural thickening with diffuse loss of normal wall layers and hypoechogenicity or mixed echogenicity of the wall, leading to luminal narrowing (10,15,18,23). Intestinal leiomyosarcoma, a mesenchymal tumor similar to GIST, usually presents as a heterogeneous intestinal mass eccentrically projecting from the bowel wall (1,5,19,22). Large tumors can contain single or multiple hypoechoic or anechoic cavitary areas accompanied by peritoneal effusion or free gas. GISTs usually exhibit an exophytic growth pattern that grows outward while preserving the GI lumen until the late stage of

the tumor (3,10,11,15,21). Owing to delayed luminal obstruction, GIST can become very large before the onset of clinical signs. Similarly, in our case, even though the large size of the tumor prevented determining its origin and its anatomical relationship with adjacent organs; there was no evidence of significant GI obstruction or clinical signs, such as vomiting, anorexia, and weight loss. This typical exophytic growth pattern is found in 79% of human patients with GISTs, although the growth patterns of GISTs can be extraluminal, intraluminal, or mixed (dumbbell-shaped) (3,11,15,19,21).

The imaging features of GI tumors vary depending on tumor size. Small tumors often have homogeneous density and regular margins, whereas large tumors tend to have irregular lobulated margins, mucosal ulceration, and heterogeneous enhancement due to necrosis, hemorrhage, or cavitation within the mass (4,5,13,19). GIST rupture can be suspected in tumors with a large size, lobulated shape, eccentric necrosis with peritonitis, hemoperitoneum or adjacent hematoma, and ascites on CT (19,22,23). In our case, the mass was large but showed a relatively homogeneous enhancement pattern without mucosal necrosis. The fat stranding and small amount of fluid was observed around the mass; however, there was no evidence of peritonitis or hemoperitoneum such as adhesion between the mass and adjacnet intestinal loops, mesenteric swelling, or effusion containging the echogenic sludge. Thus, GIST rupture was not considered, and the absence of rupture was confirmed by laparotomy.

Determining tumor origin is essential for making the surgical plan. CT identifies GI tract segments and tumor location. However, when the mass occupies most of the abdomen or involves many GI segments, identifying blood vessels can help determine tumor location, as reported for pelvic, liver, and spinal tumors (8,9,12,16). The cranial and caudal mesenteric arteries supply the colon. The cranial mesenteric artery branches into the ileocolic artery to supply the cecum; and ileocolic artery proximally and right colic artery distally to supply the ascending colon; the right colic artery proximally and middle colic artery to supply the transverse colon; and the middle colic artery to supply the proximal half of the descending colon (6). Post-contrast CT can visualize the arteries and veins supplying tumors. In our case, the GIST was found to originate in the cecum by identifying the vessels supplying the mass on post-contrast CT images.

Conclusions

This study described CEUS and CT features of a cecal GIST in a dog. CEUS and CT revealed low-contrast enhancement, indicating low blood flow to the tumor. These perfusion patterns and the exophytic growth pattern, location and extent of the tumor on CT images can be used to diagnose GIST and distinguish between GIST and other GI tumors. However, the large size of the GIST in our case may have influenced perfusion patterns. Therefore, further research is needed to characterize typical perfusion patterns in dogs with GISTs.

Source of Funding

This research was funded by Cambodia Higher Education Improvement Project (Credit No. 6221-KH).

This research is made possible by the generous support of the American People provided to the Center of Excellence on Sustainable Agricultural Intensification and Nutrition (CE SAIN) of the Royal University of Agriculture through the Feed the Future Innovation Lab for Collaborative Research on Sustainable Intensification at Kansas State University funded by the United States Agency for International Development (USAID) under Cooperative Agreement No. AID-OAA-L-14-00006. The contents are the sole responsibility of the authors and do not necessarily reflect the views of USAID or the United States Government. All budget revisions must be submitted to and approved by CE SAIN prior to utilizing funds.

Acknowledgements

The authors are grateful to Prof. Jezie Alix Acord, in the Department of Veterinary Paraclinical Sciences, College of Veterinary Medicine, University of the Philippines Los Baños, Los Baños, Laguna, Philippines for advice in drafting this manuscript.

Conflicts of Interest

The authors have no conflicting interests.

Ethical Declaration

The study was reviewed and approved by the director of Chonnam National University Veterinary Teaching Hospital.

Author Contribution

Conceptualization: Choi J; Data curation: Choi J; Formal analysis: Kim S, Choi J; Funding acquisition: Kang K; Investigation: Chhoey S, Kim S; Methodology: Choi J; Project administration: Kang K, Koe S; Software: Choi J; Supervision: Choi J; Validation: Kim S, Choi J; Visualization: Chhoey S, Choi J; Writing - original draft: Chhoey S; Writing - review & edit-

ing: Chhoey S, Kim S, Choi J.

References

1. Betts MT, Huo EJ, Miller FH. Gastrointestinal and genitourinary smooth-muscle tumors. AJR Am J Roentgenol 2003; 181: 1349-1354.
2. Cho IR, Park JC, Roh YH, Choi SI, Lee JE, Kim EH, et al. Noninvasive prediction model for diagnosing gastrointestinal stromal tumors using contrast-enhanced harmonic endoscopic ultrasound. Dig Liver Dis 2019; 51: 985-992.
3. Choi J, Kim H, Lee H, Kim J, Yoon J. Medical imaging and immunohistochemical diagnosis of gastrointestinal stromal tumor originated from colon in a dog. Korean J Vet Res 2008; 48: 111-117.
4. Cui NY, Gong XT, Tian YT, Wang Y, Zhang R, Liu MJ, et al. Contrast-enhanced ultrasound imaging for intestinal lymphoma. World J Gastroenterol 2021; 27: 5438-5447.
5. Dahlerup JF, Eivindson M, Jacobsen BA, Jensen NM, Jørgensen SP, Laursen SB, et al. Diagnosis and treatment of unexplained anemia with iron deficiency without overt bleeding. Dan Med J 2015; 62: C5072.
6. Evans HE, de Lahunta A. The digestive apparatus and abdomen. In: Evans HE, de Lahunta A, editors. Miller's anatomy of the dog. 4th ed. St Louis: Saunders. 2013: 281-327.
7. Frances M, Lane AE, Lenard ZM. Sonographic features of gastrointestinal lymphoma in 15 dogs. J Small Anim Pract 2013; 54: 468-474.
8. Gore RM, Pickhardt PJ, Mortele KJ, Fishman EK, Horowitz JM, Fimmel CJ, et al. Management of incidental liver lesions on CT: a white paper of the ACR incidental findings committee. J Am Coll Radiol 2017; 14: 1429-1437.
9. Hu HJ, Huang YW, Zhu YC. Tumor feeding artery reconstruction with multislice spiral CT in the diagnosis of pelvic tumors of unknown origin. Diagn Interv Radiol 2014; 20: 9-16.
10. Ignee A, Jenssen C, Hocke M, Dong Y, Wang WP, Cui XW, et al. Contrast-enhanced (endoscopic) ultrasound and endoscopic ultrasound elastography in gastrointestinal stromal tumors. Endosc Ultrasound 2017; 6: 55-60.
11. Irie M, Tomiyasu H, Tsujimoto H, Kita C, Kagawa Y. Prognostic factors for dogs with surgically resected gastrointestinal stromal tumors. J Vet Med Sci 2021; 83: 1481-1484.
12. Iwazawa J, Ohue S, Mitani T, Abe H, Hashimoto N, Hamuro M, et al. Identifying feeding arteries during TACE of hepatic tumors: comparison of C-arm CT and digital subtraction angiography. AJR Am J Roentgenol 2009; 192: 1057-1063.
13. Lassau N, Lamuraglia M, Chami L, Leclère J, Bonvalot S, Terrier P, et al. Gastrointestinal stromal tumors treated with imatinib: monitoring response with contrast-enhanced sonography. AJR Am J Roentgenol 2006; 187: 1267-1273.
14. Lee S, Hwang J, Kim H, Hong Y, Lee G, Chung D, et al. Computed tomographic findings may be useful for differentiating small intestinal adenocarcinomas, lymphomas, and spindle cell sarcomas in dogs. Vet Radiol Ultrasound 2023; 64: 233-242.
15. Maas CP, ter Haar G, van der Gaag I, Kirpensteijn J. Reclassification of small intestinal and cecal smooth muscle tumors in 72 dogs: clinical, histologic, and immunohistochemical evaluation. Vet Surg 2007; 36: 302-313.
16. Mascalchi M, Quilici N, Ferrito G, Mangiafico S, Scazzeri F, Torselli P, et al. Identification of the feeding arteries of spinal vascular lesions via phase-contrast MR angiography with three-dimensional acquisition and phase display. AJNR Am J Neuroradiol 1997; 18: 351-358.
17. Medellin A, Merrill C, Wilson SR. Role of contrast-enhanced ultrasound in evaluation of the bowel. Abdom Radiol (NY) 2018; 43: 918-933.
18. Montañés I, Vila A, Roura X, Santos L, Canturri A, Verdés J, et al. Gastrointestinal stromal tumors (GIST): retrospective study of 6 dogs. Clin Vet Peq Anim 2019; 39: 155-161.
19. Myers NC, Penninck DG. Ultrasonographic diagnosis of gastrointestinal smooth muscle tumors in the dog. Vet Radiol Ultrasound 1994; 35: 391-397.
20. Nisa K, Lim SY, Shinohara M, Osuga T, Yokoyama N, Tamura M, et al. Evaluation of duodenal perfusion by contrast-enhanced ultrasonography in dogs with chronic inflammatory enteropathy and intestinal lymphoma. J Vet Intern Med 2019; 33: 559-568.
21. Sandrasegaran K, Rajesh A, Rushing DA, Rydberg J, Akisik FM, Henley JD. Gastrointestinal stromal tumors: CT and MRI findings. Eur Radiol 2005; 15: 1407-1414.
22. Simeoni F, Del Signore F, Aste G, Bargellini P, Rubini G, Terragni R, et al. B-mode and contrast enhanced ultrasonography features of gastric inflammatory and neoplastic diseases in dogs. Animals (Basel) 2021; 11: 670.
23. Simeoni F, Signore FD, Terragni R, Tamburro R, Aste G, Vignoli M. Diagnostic imaging of gastrointestinal tumours in dogs and cats: a review. Am J Anim Vet Sci 2020; 15: 89-101.
24. Tanaka T, Akiyoshi H, Mie K, Okamoto M, Yoshida Y, Kurokawa S. Contrast-enhanced computed tomography may be helpful for characterizing and staging canine gastric tumors. Vet Radiol Ultrasound 2019; 60: 7-18.
25. Zuercher M, Vilaplana Grosso F, Lejeune A. Comparison of the clinical, ultrasound, and CT findings in 13 dogs with gastric neoplasia. Vet Radiol Ultrasound 2021; 62: 525-532.